Journal of Power Sources 195 (2010) 2149–2158

Contents lists available at ScienceDirect

Journal of Power Sources

journal homepage: www.elsevier.com/locate/jpowsour

The effect of HCl in syngas on Ni–YSZ anode-supported solid oxide fuel cells

Chunchuan Xu[a,*], Mingyang Gong[b], John W. Zondlo[a], XingBo Liu[b], Harry O. Finklea[c,d]

[a] Department of Chemical Engineering, West Virginia University, Morgantown, WV 26506, USA
[b] Department of Mechanical & Aerospace Engineering, West Virginia University, Morgantown, WV 26506, USA
[c] C. Eugene Bennett Department of Chemistry, West Virginia University, Morgantown, WV 26506, USA
[d] National Energy Technology Laboratory-Institute for Advanced Energy Studies, US Dept. of Energy, USA

ARTICLE INFO

Article history:
Received 5 August 2009
Received in revised form
20 September 2009
Accepted 30 September 2009
Available online 17 October 2009

Keywords:
SOFC
Ni–YSZ anode
Coal syngas
HCl impurity
Nickel morphological change
Chlorine adsorption

ABSTRACT

The Ni–YSZ cermet anode of the solid oxide fuel cell (SOFC) has excellent electrochemical performance in a clean blended synthetic coal syngas mixture. However, chloride, one of the major contaminants existing in coal-derived syngas, may poison the Ni–YSZ cermet and cause degradation in cell performance. Both hydrogen chloride (HCl) and chlorine (Cl_2) have been reported to attack the Ni in the anode when using electrolyte-supported SOFCs. In this paper, a commercial anode-supported SOFC was exposed to syngas with a concentration of 100 ppm HCl under a constant current load at 800 °C for 300 h and 850 °C for 100 h. The cell performance was evaluated periodically using electrochemical methods. A unique feature of this experiment is that the active central part of the anode was exposed directly to the fuel without an intervening current collector. Post-mortem analyses of the SOFC anode were performed using X-ray diffraction (XRD), scanning electron microscopy (SEM), energy dispersive spectroscopy (EDS) and X-ray photoelectron spectroscopy (XPS). The results show that the 100 ppm concentration of HCl causes about 3% loss of performance for the Ni–YSZ anode-supported cell during the 400 h test. Permanent changes were noted in the surface microstructure of the nickel particles in the cell anode.

1. Introduction

A Ni–YSZ cermet anode-supported SOFC can directly use coal-derived syngas because of its ability to tolerate the CO and CO_2 which are present in the syngas. However, the presence of volatile contamination containing P, S, Cl, As, Sb, Cd, Be, Se, Pb, and Hg species in warm syngas can cause degradation of the SOFC performance [1]. A high level of chloride ranging from 0.01% to 0.5% is found in U.S. coals and these chlorides will be converted into HCl during the gasification process [2]. After water scrubbing of the coal-derived syngas, there still remains a significant amount of the HCl present in gas phase. To investigate the HCl tolerance of the SOFC, Trembly et al. tested a Ni–YSZ anode in an electrolyte-supported cell using syngas with 20 ppm and 160 ppm HCl. Their results showed that the degradation in cell performance was over 17% and 26% in 100 h, respectively. However, there was no trace of $NiCl_2$ on the cell following ex situ chemical examination. Adsorption of chlorine onto the Ni to reduce the triple phase boundary (TPB) was postulated as one possible explanation [2]. Haga et al., by using both Cl_2 and HCl in H_2 fuel, reported significant degradation of a Ni–YSZ anode electrolyte-supported cell. They proposed that the reaction of Cl_2 with Ni could form a gas phase nickel chloride ($NiCl_2$) which causes a loss of Ni concentration in Ni–YSZ anode [3]. HCl is the one of the most stable chloride phases in the SOFC fuel system. The reaction between HCl and Ni is not thermodynamically favored over 450 °C [4]. The adsorption of chlorine onto Ni particles in the cell anode and the loss of nickel concentration have both been postulated as the cause of the cell degradation, but there still remain unanswered questions about the nature of HCl poisoning of the SOFC.

In this paper, a commercial Ni–YSZ anode-supported cell was used for testing. The thick cell anode can possibly enhance measurable chemical and structural changes of the nickel. Periodic evaluation of impedance follows the ohmic and polarization resistances during the experiment. Extensive post-mortem analyses by SEM, XRD, and XPS are used to evaluate chemical and structural changes in the anode.

2. Experimental methods

2.1. SOFC composition and test set-up

In this study, commercial anode-supported solid oxide button cells manufactured by Materials and Systems Research Inc. (MSRI) were tested. The cells consisted of five layers: (1) about 0.8–0.9 mm

* Corresponding author at: Department of Chemical Engineering, West Virginia University, Morgantown, WV 26506-6102, USA. Tel.: +1 304 293 9379; fax: +1 304 293 4139.
E-mail address: Chunchuan.Xu@mail.wvu.edu (C. Xu).

0378-7753/$ – see front matter © 2009 Elsevier B.V. All rights reserved.
doi:10.1016/j.jpowsour.2009.09.079

thick Ni–8YSZ layer which supports the cell structure, (2) 25-μm thick highly catalytic Ni–8YSZ mixture interlayer, (3) 20-μm thick 8YSZ (YSZ) electrolyte, (4) 25-μm thick $La_{0.8}Sr_{0.2}MnO_3$ (LSM)–8YSZ interlayer, and (5) 50-μm thick current collection layer made of LSM. The cell effective area (cathode side) is 2 cm^2 [5]. The cell contact configuration has been described in an earlier paper [6]. Using this special contact configuration, the central portion of the anode was directly exposed to the injected fuel without any intervening current collector or metal paste so that the impurity effects on the cell anode can be readily observed and identified. Mass flow controllers were employed to control the flow rates of H_2, CO, CO_2, N_2/HCl (5000 ppm HCl in a balance of nitrogen) and air separately. A temperature-controlled humidifier was used to adjust the H_2O concentration of the simulated coal syngas fed to the anode. The total syngas fuel flow rate was kept constant at approximately 200 ± 2 standard cubic centimeters per minute (sccm) and the air-flow rate was held at approximately 300 ± 2 sccm. The anode fuel transfer lines were heat-traced to over 120 °C so that water condensation between the humidifier and furnace was prevented. CO, CO_2 and HCl were injected downstream of the anode humidifier close to furnace into a ceramic (Al_2O_3) inlet tubing to ensure that all trace species in the stream reached the anode of the SOFC in a minimum amount of time.

2.2. Electrochemical testing of the SOFC

The "as-received" SOFC was heated from room temperature to 800 °C at a rate of 7 °C min^{-1}. During the heating period, the anode was provided 100 sccm of N_2 and the cathode was provided 100 sccm of air. Once the furnace temperature reached 800 °C, the anode was reduced by providing fuel flow containing 10% H_2 and the balance N_2 for approximately 2 h. After this time, 50% H_2 and 50% N_2 were fed for another hour in order to complete the reduction. The cell open circuit voltage at this point was stable at 1.065 ± 0.001 V with humidified H_2 (3% H_2O) as the fuel. The open circuit voltage (OCV) was less than the theoretical value of 1.102 V with 97% H_2, 3% H_2O on the anode side and air (21% O_2) on the cathode side presumably because of slight leakage around the cell seals and possibly through the electrolyte. Then, 0.25 A cm^{-2} direct current (DC) was loaded for a current treatment overnight (14 h). The constant DC current density load was supplied by a solid-state load cell (TDI Transistor Devices SDL-1103). Upon loading the SOFC at constant current density of 0.5 A cm^{-2} for another 2 h, the cell voltage stabilized at 0.725 ± 0.001 V. After shifting to syngas fuel (30% H_2, 26% H_2O, 23% CO, and 21% CO_2), the cell OCV decreased to 0.942 ± 0.003 V. This value is close to the theoretical OCV of 0.947 V with 30% H_2, 26% H_2O and the theoretical OCV 0.949 V with 23% CO, 21% CO_2 at the anode and air at cathode. After the cell voltage stabilized at 0.625 ± 0.003 V under a loading current density of 0.5 A cm^{-2} for 115 h, 100 ppm HCl was injected into the fuel stream downstream from the humidifier just before entering the furnace. After exposure to syngas with 100 ppm HCl for 300 h, the cell temperature was increased from 800 °C to 850 °C with the HCl still present. The cell voltage increased to 0.675 ± 0.003 V under a load of 0.5 A cm^{-2}. The cell OCV dropped to 0.925 ± 0.003 V, which is lower than the theoretical OCV 0.932 V with 30% H_2, 26% H_2O at anode and air at cathode and equal to the theoretical OCV 0.925 V with 23% CO, 21% CO_2 at anode and air at cathode. The cell ran continually for 100 h at 850 °C before cutting off the flow of the HCl impurity. The cell polarization curves and impedance spectra were taken at 10 h, 70 h, 107 h, 150 h, 195 h, 250 h and 300 h at 800 °C, and at 10 h, 50 h, and 100 h at 850 °C after adding HCl. The impedance spectra were collected using a Solartron SI 1260 impedance/gain-phase analyzer with an AC amplitude of 20 mV at frequencies ranging from 100 kHz to 0.1 Hz. The WE and RE2 leads were connected to the cell cathode current collection and voltage leads respectively; the CE and RE1 leads were connected to the cell anode current collection and voltage leads respectively. Exhaust water samples were condensed and collected periodically after adding the HCl impurity in the fuel. During the cell cool down period, the anode side of cell was purged with N_2 to quench any reactions. Cool down to room temperature required about 3 h. A 6 mm × 4 mm size post-mortem sample of the central area of the cell was cut and well polished for EDS chemical analysis.

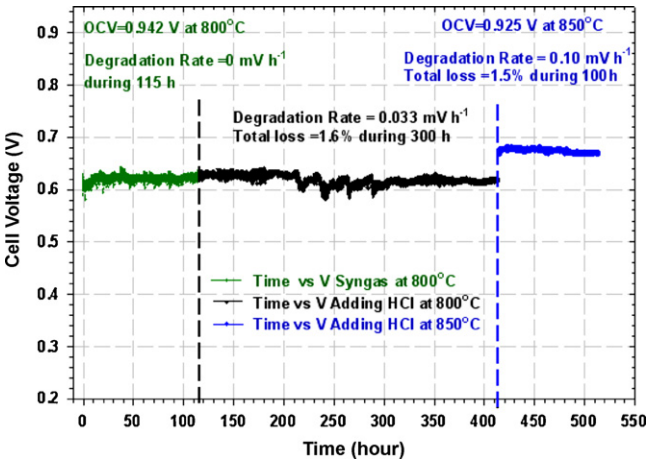

Fig. 1. The cell was stabilized after exposure to clean syngas for 115 h, then 100 ppm HCl was added for 400 h. The cell voltage drop is about 10 mV in the first 300 h at 800 °C, and 10 mV in the next 100 h at 850 °C.

2.3. Morphology, structural and chemical analysis

The microstructure and chemical composition of the cell anode were examined with a Hitachi S-4700 SEM/EDS. To determine the composition of the anode, XRD (Panalytical X'Pert PM-3040 PRO) with a Cu K-alpha radiation source (1.54060 Å), and XPS (PHI 5000 VerasProbe XPS Microprobe) with a monochromatic Al K-alpha radiation source (8.34118 Å) were employed. Thermodynamic analysis was carried out with the FACTSAGE 5.4 software package to predict the predominant phase behavior under the operating conditions of the experiment by calculating the minimum Gibbs free energy change of the proposed reactions.

3. Results

3.1. Polarization curves and impedance spectra

After the application of 200 sccm simulated syngas, the cell OCV gradually stabilized at 0.942 V and the cell voltage was about 0.620 ± 0.005 V under a constant current load of 0.5 A cm^{-2}. The cell performance (voltage at a constant current density) was stable for over 115 h in coal syngas. Upon the introduction of 100 ppm HCl at hour 115, the cell voltage remained unchanged for about the next 100 h (Fig. 1). The fluctuations of voltage between 200 h and 300 h were caused by drops in the lab room temperature (the room temperature once dropped to 9 °C from 21 °C accidently which led to the cell voltage fluctuation). At a constant current load of 0.5 A cm^{-2}, the cell voltage began to decrease around hour 200 with an average degradation rate of about 0.033 mV h^{-1} at 800 °C. At 850 °C, the cell showed a greater degradation in performance with an average degradation rate of 0.1 mV h^{-1}. The cell OCV consistently remained at 0.942 V at 800 °C and 0.925 V at 850 °C. The loss of cell performance was not significant as seen over nearly all current densities (Fig. 2). At the diffusion limited region near zero cell voltage, the variations about ±0.1 A cm^{-2} over the testing period were not related to the time after the addi-

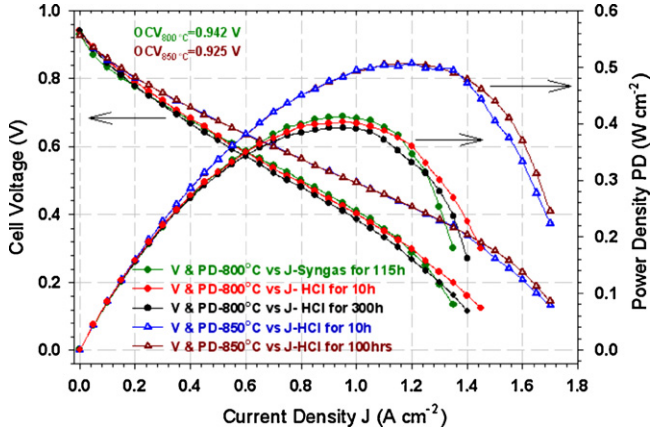

Fig. 2. The polarization and power density curves for the SOFC exposed to syngas with 100 ppm HCl impurity for 400 h. The overlapping polarization and power density curves at different times for a given temperature demonstrate insignificant changes of cell performance.

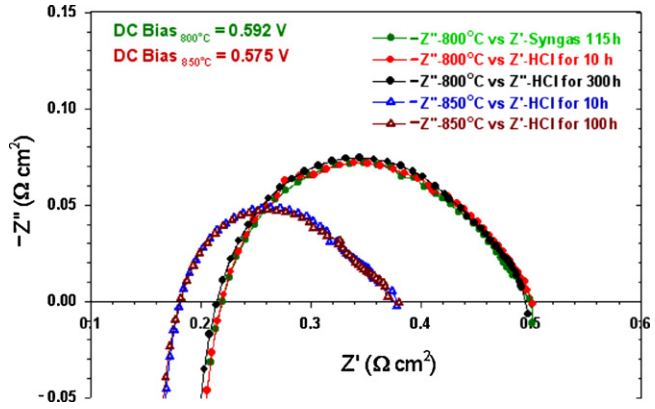

Fig. 3. The normalized impedance curves during 400 h of operation in 100 ppm HCl impurity at 800 °C and 850 °C.

tion of HCl. This variation possibly came from the change of the environment, such as the room temperature and ambient pressure.

The impedance spectra under a DC bias of 0.592 V (equivalent to a DC potentiostatic load of 0.350 V) at 800 °C (Fig. 3) show that the series resistances, R_s (high frequency intercept with the

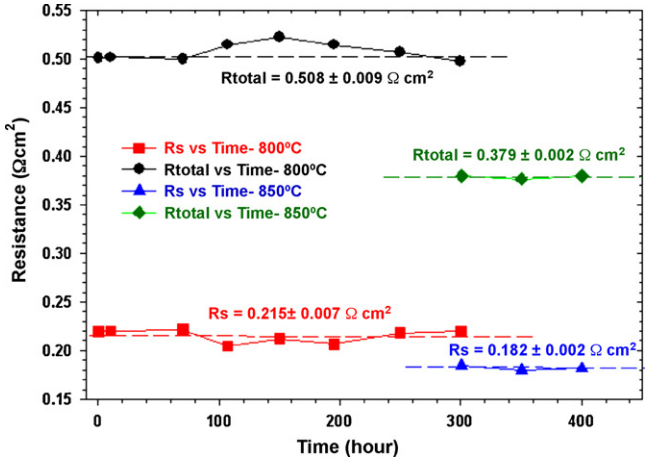

Fig. 4. The measured series and total polarization resistances are nearly constant with time. The variations of these resistances exhibit no trend with respect to the time of exposure to 100 ppm HCl in both the 800 °C and 850 °C cases.

Z' axis), vary between 0.210 Ω cm^2 and 0.220 Ω cm^2 with a mean of 0.215 Ω cm^2. The total polarization resistances, R_{total} (low frequency intercept with the Z' axis) vary between 0.500 Ω cm^2 and 0.510 Ω cm^2 with a mean of 0.507 Ω cm^2. Under a DC bias of 0.575 V at 850 °C, the variations of both R_s and R_{total} are less than 0.004 Ω cm^2 with means of 0.182 Ω cm^2 and 0.378 Ω cm^2 respectively. The variation of measured R_s and R_{total} did not reflect a trend related to the application of 100 ppm HCl in both the 800 °C and 850 °C cases (Fig. 4). These small variations of R_s and R_{total} come from measurement system errors.

3.2. SEM micrographs and EDS spectra

Photographs of the anodes for a clean reduced cell and the HCl-poisoned cell are shown in Fig. 5(a) and (b) respectively. Despite a few brown rust particles which fell from the corroded stainless steel fitting in the fuel exhaust, the HCl-exposed anode surface in Fig. 5(b) shows a uniform appearance of the reduced Ni–YSZ cermet comparable to the clean reduced cell anode in Fig. 5(a). The cell anode cross-section and top surface SEM images of a clean reduced cell in Fig. 6(a) and (c) are provided for comparison to those of the cell exposed to HCl in Fig. 6(b) and (d). The HCl-poisoned anode does not show significant changes of pore structure at the micron level. However, some differences can be found in the 50K magnification

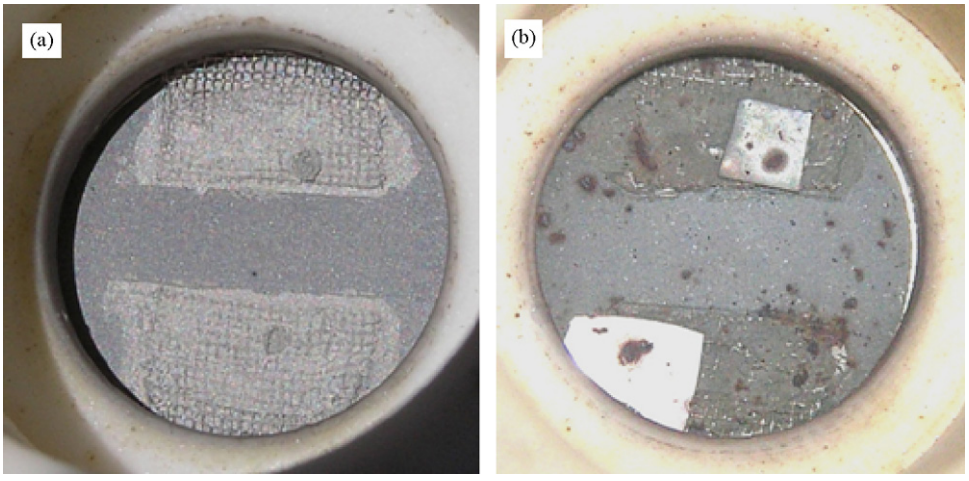

Fig. 5. The comparison of anode surfaces (a) for the clean reduced cell and (b) for the cell after exposure to syngas with 100 ppm HCl for 400 h. The brown spots are from rust which fell from the stainless steel exhaust tubing attacked by HCl.

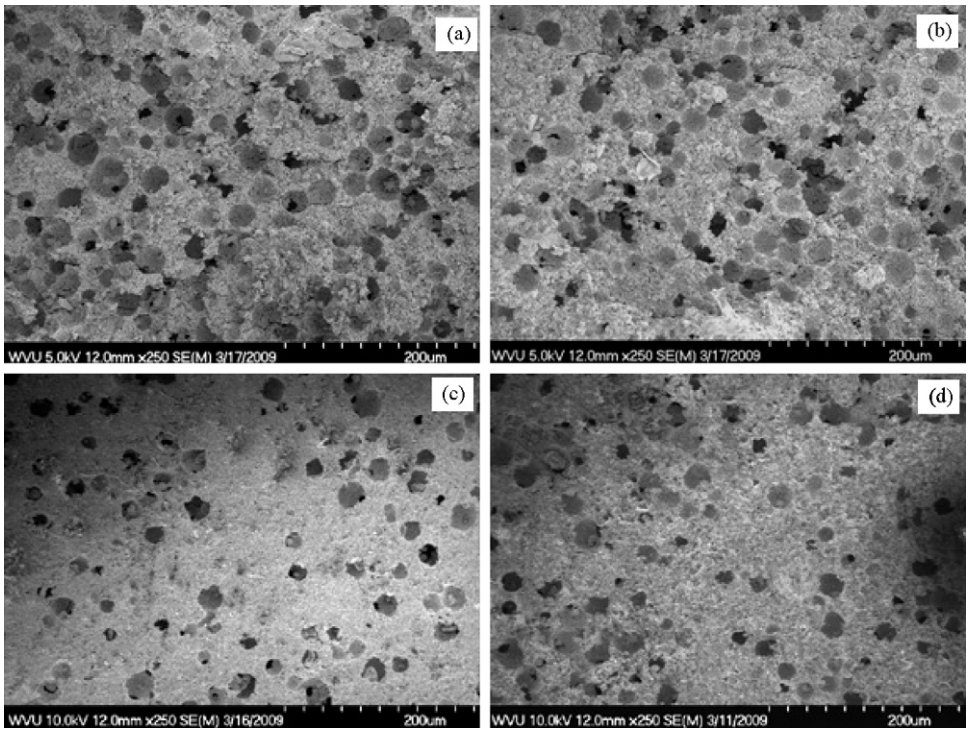

Fig. 6. The SEM micrographs of a clean reduced cell cross-section (a) and anode surface (c) compared to that of the cell (b) and (d) after exposure to syngas with 100 ppm HCl for 400 h.

micrographs shown in Fig. 7. The images of the anode cross-section near the interface region in Fig. 7(a) and top surface Fig. 7(c) for the clean reduced cell show that the surfaces of YSZ and Ni particles are smooth and indistinguishable without EDS chemical analysis. Similar images of the HCl-poisoned cell in Fig. 7(b) and (d) show that the surface of the Ni particles took on a rough texture that is readily evident. The same phenomena are observed over the entire Ni–YSZ anode exposed surface and cross-section. Comparing the cross-sectional interface image, Fig. 7(b), to that of the top anode surface, Fig. 7(d), the Ni particles on the exposed anode surface are more scabrous than those at the interface. The particle size of the Ni and YSZ is about 1–3 μm as seen from the SEM images. The changes

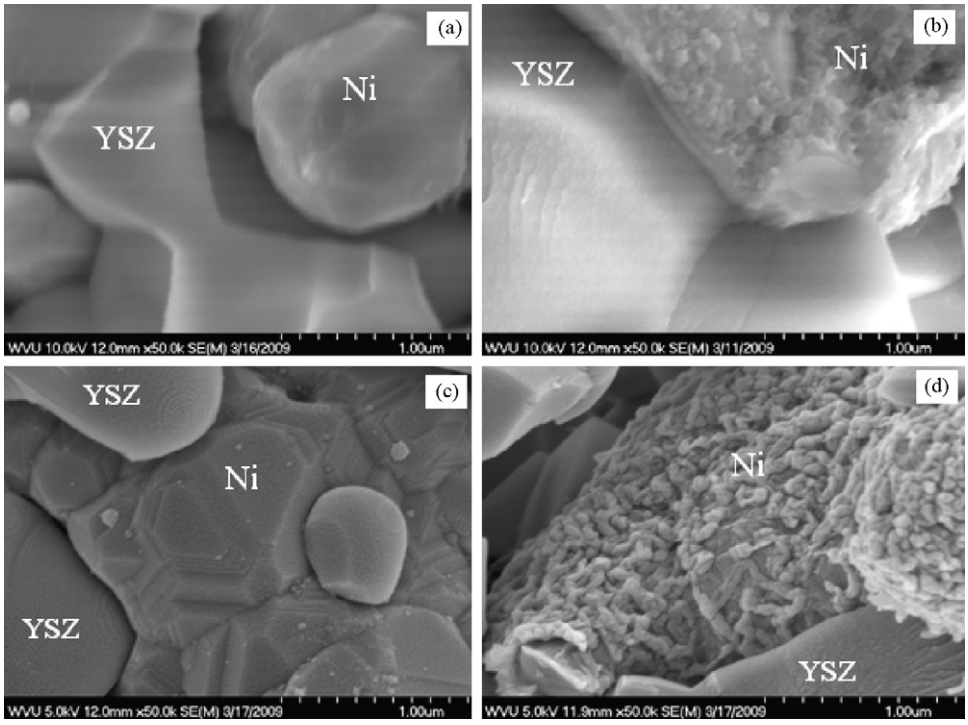

Fig. 7. Detailed SEM micrographs at 50K magnification of the clean reduced cell near the interface section (a) and the top surface (c) compared to those of the cell (b) and (d) after exposure to syngas with 100 ppm HCl for 400 h.

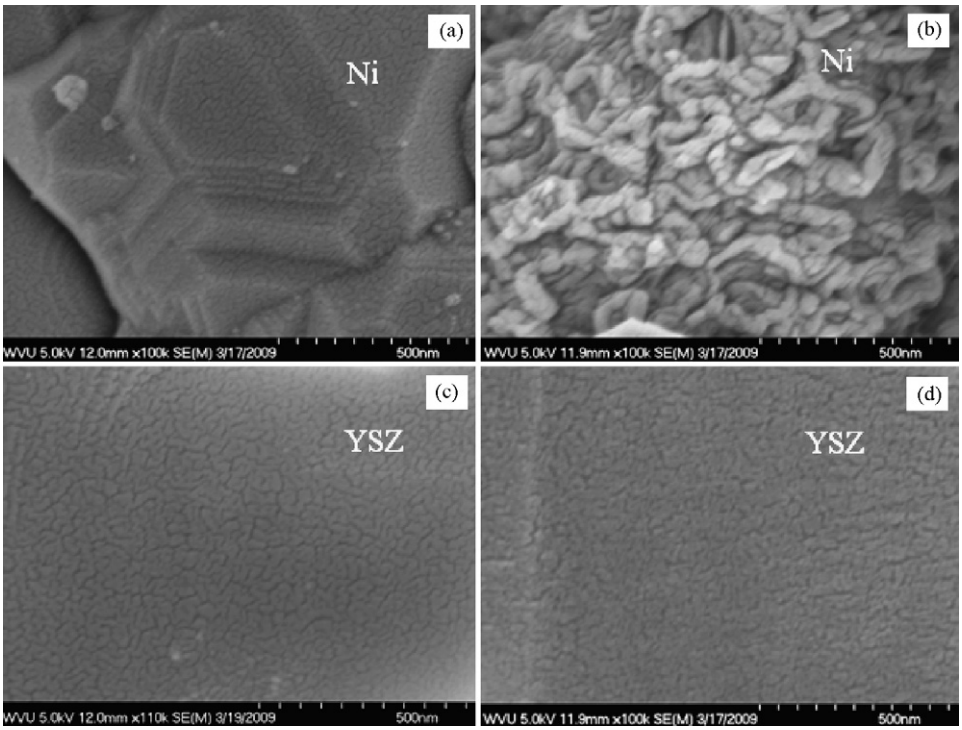

Fig. 8. The SEM micrographs with 100K magnification showing the Ni (a) and the YSZ particles of a clean reduced cell anode (c) compared to those of the cell (b) and (d) after exposure to syngas with 100 ppm HCl for 400 h.

of the Ni particles on the surface can be clearly shown in the 100K magnification micrographs in Fig. 8(a) and (b), but the texture of the YSZ particles on the surface has no notable change as in Fig. 8(c) and (d). Although the electrochemical measurements did not reveal significant loss of cell performance, the surface microstructure of the Ni anode catalyst was altered at the submicron level.

The EDS spectra (with 10 keV incident electron beam energy) of the clean unpolished reduced anode and the HCl-poisoned anode display detectable amounts of Ni, Y, Zr, and O as shown in Fig. 9(i). There is no detectable Cl signal on the HCl-poisoned anode surface. The peak intensities of Ni and YSZ are almost equivalent between the clean and poisoned samples. Because the unpolished cell surface involves large EDS measurement errors, a 6 mm × 4 mm size sample of the central area of both the clean and HCl-poisoned cells were cut and well polished under the same polishing conditions typical for EDS chemical analysis. The polished clean and poisoned samples lost about 20 μm in thickness from the top anode surfaces after polishing. With 20 keV incident electron energy, the EDS spectra in Fig. 9(ii) show that all Ni peak intensities of the poisoned anode are relatively lower than those of the clean anode. The EDS results suggest that the amount of Ni for the poisoned anode was reduced by about 2% of the total of Ni–YSZ weight, compared to that of the clean anode. The Si signal at 1.75 keV came from the polishing paste which got trapped in the pores during polishing. There is a weak Fe signal appearing in the poisoned EDS spectrum. The Fe signal comes from the particles of the corroded stainless steel fitting which remained in the pores of the Ni–YSZ matrix (see Fig. 5).

Table 1
XRD peak list by $2\theta^{\circ}$.

YSZ peaks [7]	Ni peaks [8]	NiO peaks [9]
30.10°	44.17°	37.24°
34.89°	51.49°	43.27°
50.21°		62.59°
59.79°		
62.86°		

To check the exhaust gas composition, the condensed exhaust water was collected for chemical analysis. The condensed exhaust water from the cell outlet was light brown in color and had a pH value of about 2.7–3.5. Silver nitrate ($AgNO_3$) was used to precipitate the Cl and verify its presence in the exhaust water. Evaporation of the collected water left a solid residue showing a slight greenish color. The EDS spectrum of this dehydrated residue revealed detectable trace elements including Cl, Fe, Cr, Ni, Na, C, O and Au (Fig. 10). The gold (Au) was used to coat the sample surface for better SEM imaging. The high Cl intensity indicates that the 100 ppm HCl impurity passed through the anode side of the cell and carried with it trace elements such as Fe, Cr, Ni, and Na. The traces of C and O may be from the fuel mixtures. According to ASTM A269-08, the SX 316 series stainless steel tubing is composed of Fe, Cr (16–18%), Ni (10–16%) and Mo (2–3%). The significant Fe and Cr concentrations in the exhaust water provide evidence that the HCl attacked the stainless steel fitting and tubing as it emerged hot from furnace in the exhaust. Thus, it is not a surprise to see the brown stains of iron oxide on the surface of post-mortem cell anode in Fig. 5. These particles apparently fell down through the anode exhaust tubing and collected on the cell anode surface. The Mo signal at 2.29 keV is too weak or may be hidden by the Au peak.

3.3. XRD and XPS analyses

XRD analysis was conducted on the cell after exposure to 100 ppm HCl with syngas. There is no detectable signal due to metal chloride-containing phases in the XRD spectra Fig. 11(a). The peak positions of YSZ, Ni, NiO are listed in Table 1 by 2θ locations [7–9]. Comparison of the spectrum for the clean anode, Fig. 11(b), and the HCl-poisoned anode, Fig. 11(a), reveals that the two spectra are virtually identical. This observation indicates that the basic microscopic structure of Ni–YSZ did not change in the cell after exposure to syngas with 100 ppm HCl. This result also agrees with the results of Trembly et al. [2]. The spectra of an HCl-poisoned YSZ coupon and a clean YSZ sample are identical as well (Fig. 11(c) and (d)). Spectra

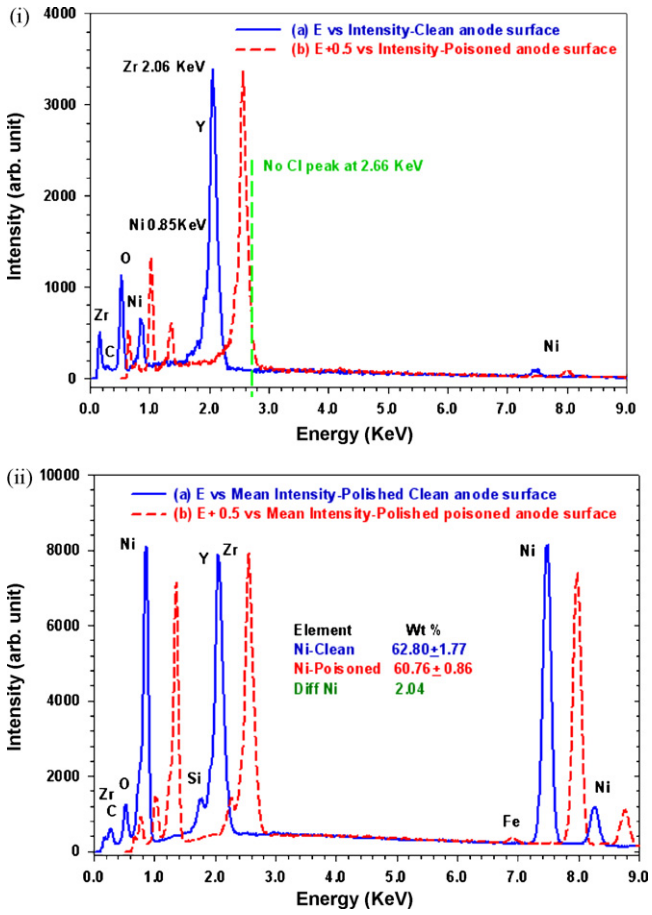

Fig. 9. (i) EDS spectra (10 keV incident electron beam energy) of the unpolished clean (a) and poisoned (b) cell anode surfaces (offset by 0.5 keV for clarity) show almost equivalent Ni and YSZ peaks intensity. A Cl signal does not appear in the spectrum of the poisoned cell. (ii) EDS spectra (20 keV electron beam energy) of the polished clean (a) and poisoned (b) cell anode surfaces (offset by 0.5 keV for clarity) show almost equivalent YSZ peak intensity. The Ni peak intensity of poisoned sample is slightly lower than that of the clean sample. A Cl signal does not appear in the spectrum of the poisoned cell.

of both an HCl-poisoned Ni coupon and a pure Ni foil have major Ni peaks at 44.17° and 51.49° in Fig. 11(e) and (f). The HCl-poisoned coupon also shows two weak NiO peaks at 37.24° and 43.27°. Thus, the spectra of the YSZ and Ni structures in the Ni–YSZ anode are consistent with those of the respective pure coupons.

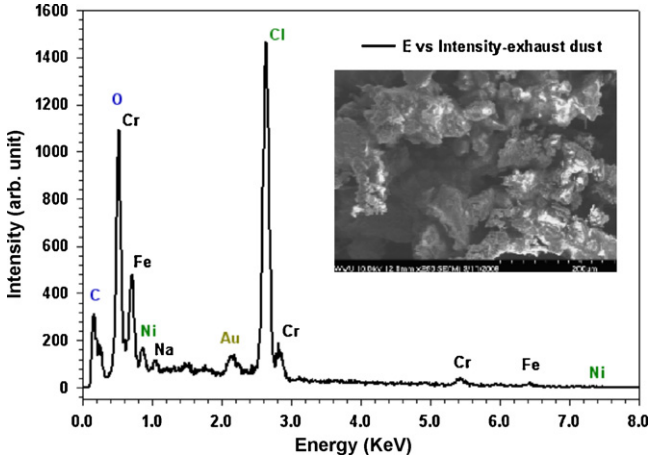

Fig. 10. The EDS spectrum and SEM image of the dehydrated residue from the exhaust water which collected at the gas outlet after adding 100 ppm HCl.

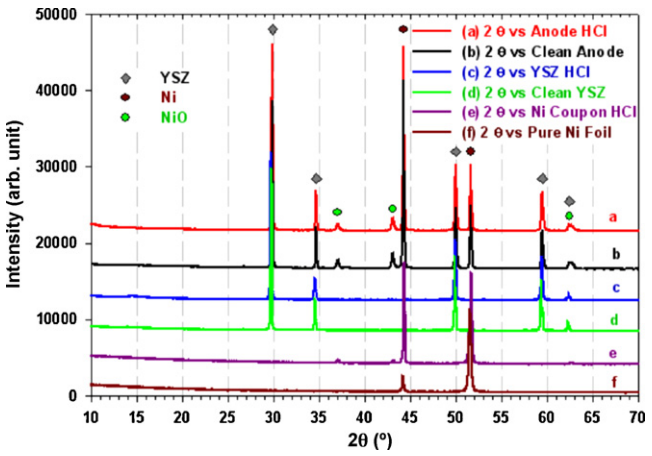

Fig. 11. XRD spectra of the HCl-exposed anode (a) and an HCl-exposed YSZ coupon (c) surfaces do not show any extra peaks when compared with a clean reduced anode (b) and a clean YSZ sample (d). The spectra of the HCl-exposed Ni coupon (e) with weak NiO peaks differs very slightly from that of pure Ni foil (f).

The XPS spectrum of the cross-section of the HCl-poisoned anode is shown in Fig. 12, after having been exposed to syngas with HCl for 400 h The major detected core level peaks are Cl_{2p}, $Zr_{3s,3p,3d}$, $Y_{3d,3p,4s}$, C_{1s}, O_{1s}, Ni_{2p} and Ni_{LMM}. The broad and weak Cl_{2p} band is associated with the peak position at 197.20 eV. The peak position of chlorine on the Ni–YSZ cermet is shifted down by about 2 eV compared to 199.20 eV [10] of the nickel chloride ($NiCl_2$) peak of the dehydrated exhaust residue in Fig. 13(c). This comparison suggests that the chlorine is in the form of adsorbed chlorine on the anode rather than that of a nickel chloride compound. This evidence implies that the chlorine is present on the cell anode by chemisorption. The $Ni_{2p3/2}$ peak at 854.20 eV is assigned to nickel oxide [11]. The peak at 157.25 eV belongs to $Y_{3d3/2}$ state of Y_2O_3 phase and the peak at 182.15 is attributed by ZrO_2 of the $Zr_{3d3/2}$ state [12]. The presence of the Y and Zr peaks provides additional evidence that YSZ has not been altered after exposure to HCl. All of these peaks also appear in the spectrum of the poisoned anode top surface. The XPS spectra results from the sample of the HCl-poisoned anode agree with those from the anode cross-section. The XPS spectra of the pure nickel and YSZ coupons which were exposed to HCl are provided as references. There are no detectable Cl peaks on either the nickel or YSZ coupon surfaces in Fig. 13(d) and (e).

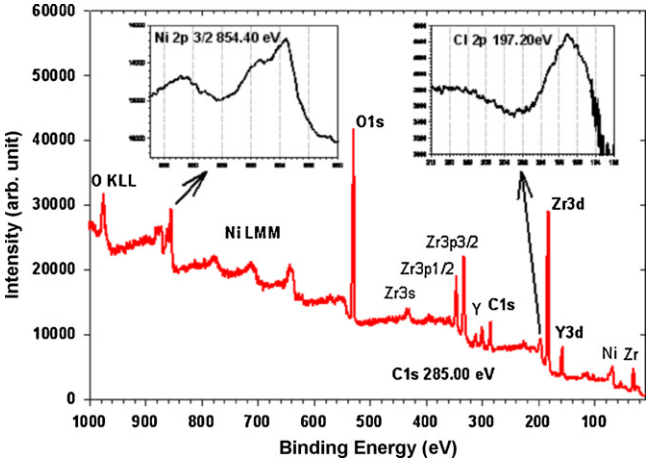

Fig. 12. XPS spectra of the HCl-poisoned anode cross-section. The presence of trace elements agrees with the EDS spectra except for a Cl peak at 197.20 eV. The peaks of $Ni_{2p3/2}$ are at 854.40 eV and 856.15 eV.

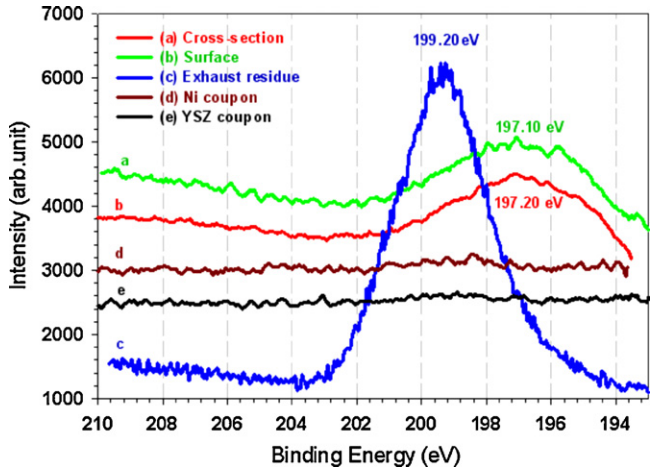

Fig. 13. The XPS Cl peak positions observed on the poisoned anode cross-section (a) and surface (b) are at 197.10 eV and 197.20 eV which is about 2.00 eV lower than that of the dehydrated exhaust residue. The XPS of the Cl peak at 199.20 eV in (c) is assigned to Fe, Cr and Ni chloride. There are no significant Cl_{2p} signals on the HCl-exposed Ni (d) and YSZ (e) coupons.

The XPS spectrum of the recovered dried solids from the condensed water can be used to identify the major elements in Fig. 14, and the relevant binding energy assignments are given in Table 2. The Cl_{2p} peak is seen at 199.20 eV. A $Cr_{2p3/2}$ peak is found at 577.40 eV which matches that of $CrCl_3$ [13]. The Fe_{2p} peak at 710.90 eV and Ni_{2p} peak at 856.50 eV are associated with $FeCl_2$ and $NiCl_2$ phases, respectively [10,13,14]. The source of Ni, Fe and Cr in the exhaust water can only be ascribed to the corrosion products from the stainless steel tubing used to carry the HCl-laden exhaust gas. The SX 316 series stainless steel exhaust tubing was corroded and broken in two places during the 400 h test as seen in Fig. 15.

4. Discussion

4.1. Cell electrochemical performance analysis

The consistency of a cell's performance can be basically evaluated by observing the series resistance, R_s, and total polarization resistance, R_{total}, when the cell was held at constant voltage under certain periods of testing. Moreover, the polarization curves and the cell power density under constant load also reflect consistent cell performance. During testing, the cell OCVs were very stable at values of 0.942 ± 0.002 V for 800 °C and 0.925 ± 0.002 V for 850 °C. Using AC impedance measurements, the measured series resistance R_s, was $0.215 \pm 0.007\ \Omega\,cm^2$ at 800 °C

Table 2
XPS binding energy peak[a] summary table.

Sample	Cl_{2p} peak	Ni_{2p} peak	Zr_{3d} peak	Y_{3d} peak	Fe_{2p} peak	Cr_{2p} peak
Anode cross-section	197.20 eV	854.40 eV	182.15 eV	157.25 eV		
Anode surface	197.10 eV	854.65 eV	182.80 eV	157.20 eV		
Ni coupon	Undetectable[b]	854.60 eVs				
YSZ coupon	Undetectable[b]		182.50 eV	157.50 eV		
Exhaust dust	199.20 eV	856.50 eV			710.90 eV	557.40 V

[a] All peaks have been calibrated with C_{1s} peak at 285.00 eV.
[b] There is no significant peak.

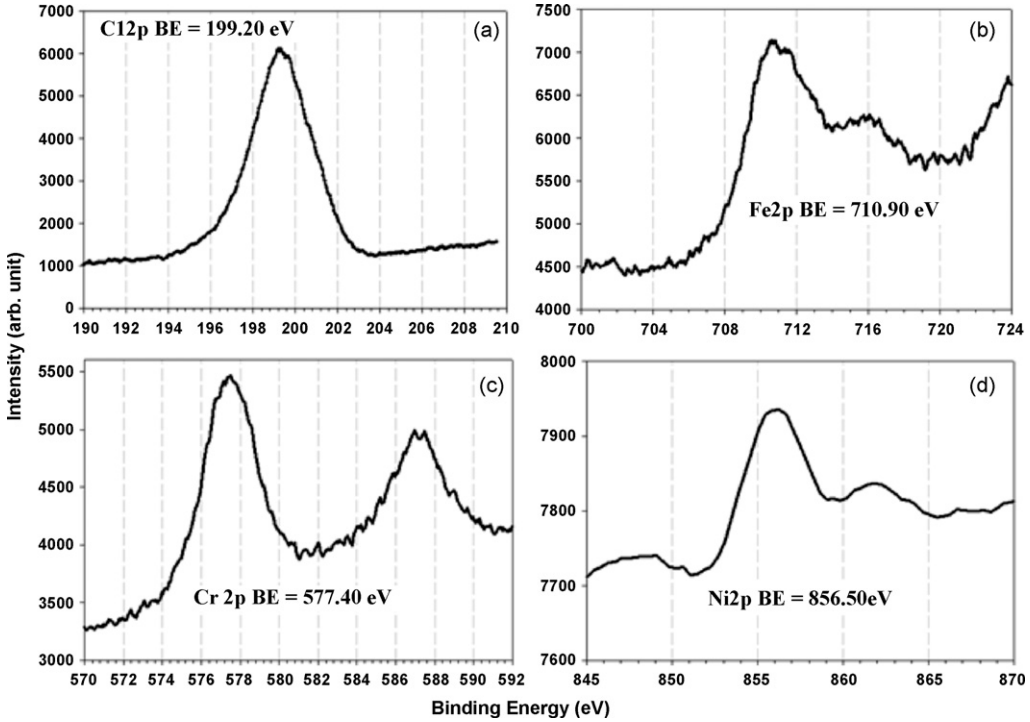

Fig. 14. XPS spectrum of the dried solids collected from the condensed water from the anode exhaust: (a) Cl_{2p} peak BE = 199.20 eV, (b) Fe_{2p} BE = 710.90 eV, (c) Cr_{2p} BE = 577.40 eV, and (d) Ni_{2p} BE = 856.50 eV.

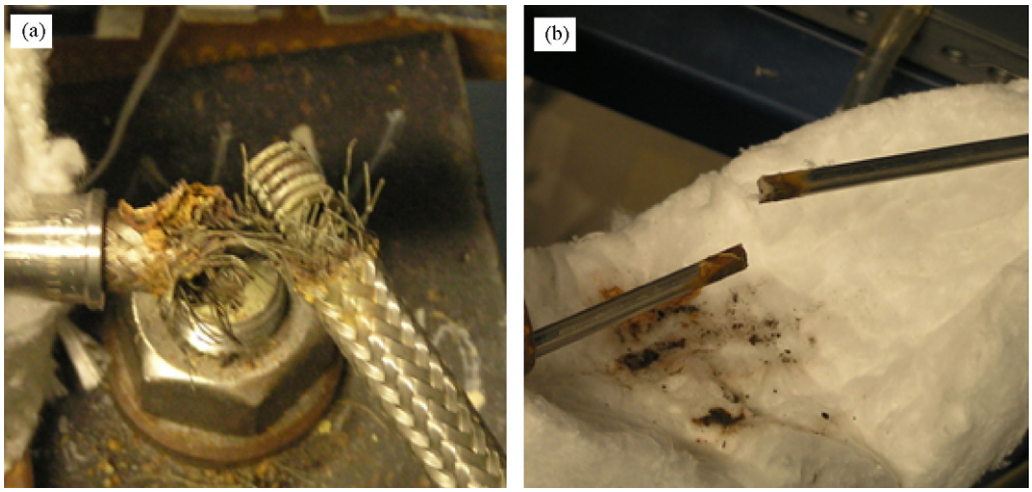

Fig. 15. The anode exhaust outlet stainless steel tubing was corroded and broken in two places during the 400 h test using syngas with 100 ppm HCl impurity.

and $0.182 \pm 0.002\ \Omega\ cm^2$ at 850 °C, the total polarization resistance, R_{total}, was $0.507 \pm 0.009\ \Omega\ cm^2$ at 800 °C and $0.378 \pm 0.002\ \Omega\ cm^2$ at 850 °C. These resistances remained nearly constant over the entire 400-h period after 100 ppm HCl was applied (Fig. 4). Although the cell did lose about 3% of voltage in total under constant current load during the 400 h, the electrochemical impedance and polarization measurement results did not show any degradation of cell performance. The impedance changes resulting from the cell voltage loss are too small to be detected accurately by the electrochemical measurements. However, some microstructural changes of the nickel were noted at high magnification in the SEM. Hence the catalysis of the nickel in the anode might even be improved because the active surface area of the nickel in contact with the syngas appeared to increase after exposure to 100 ppm HCl impurity. Although electrochemical measurement showed the overall electrode kinetics was not significantly influenced, SEM and XPS findings did suggest that some interaction between Ni–YSZ anode and HCl impurity occurred through chlorine chemisorption resulting in a morphological change of the Ni particle. For long-term operation of an SOFC with coal-derived syngas, this may pose a potential threat to cell performance. EDS analysis suggested about 2% loss of nickel weight during the 400 h of testing time. If the 0.5% sensitivity of the EDS system and the measurement error of 1.77% are taken into account, the measured 2% difference may not indicate significant loss of nickel in the anode. For the anode-supported cell tested here, the original nickel weight concentration is about 63%. The loss of about 2% nickel may not significantly impact the conductivity and catalysis of the Ni–YSZ anode. However if the nickel content continued to drop with testing time, an increase of R_s and R_{total} for the anode-supported cell may occur over longer test periods.

The impurity HCl along with the CO and CO_2 were blended dry in gas phase before mixing with wet H_2 in the ceramic tubing placed in high temperature zone at the inlet to the SOFC anode. There is no corrosion of the stainless steel inlet tubing noted prior to the HCl-laden syngas arriving at the cell anode. Thus the $NiCl_2$, $FeCl_2$ and $CrCl_3$ which were found in the anode exhaust did not interfere with the cell operation or appear as contaminates at the anode. The stainless steel tubing at the anode exhaust is outside the high temperature zone where the gas was cooled to room temperature. Thus an aqueous HCl phase was present at this point in the anode exhaust and caused the eventual corrosion of the stainless steel tubing there. This in turn resulted in the presence of the Ni, Fe and Cr chlorides in the condensed water in the exhaust stream.

4.2. Thermodynamic and phase transition analyses

In previous sections, materials analysis did not detect any secondary phase formation and AC impedance of the anode-supported cell changed only slightly after HCl exposure. Micro-morphological changes of the Ni particles as well as small losses of cell operation voltage with current load were noted, and may indicate the onset of cell degradation by HCl. Thus, a thermodynamic analysis was carried out to gain more insight into the potential reactions between HCl and the Ni–YSZ anode. Earlier studies indicated that possible reactions of Ni with HCl at SOFC working conditions mainly involved chemisorption of HCl on Ni and chlorination of the Ni surface, which can be represented by Eqs. (1) and (2) respectively as:

$$2HCl\,(g) \overset{Ni}{\rightleftarrows} 2Cl\,(ads) + H_2\,(g) \quad (1)$$

$$Ni + 2HCl \rightleftarrows NiCl_2\,(s) + H_2\,(g) \quad (2)$$

With 100 ppm concentration of HCl, the calculated Gibbs free energy change for reaction (2) at the cell working condition (1073 K, $P(H_2) = 0.3$ atm) is $+240.2\ kJ\ mol^{-1}$. Thus formation of bulk secondary nickel chloride is quite energetically unfavorable. Further thermodynamic calculation was carried out using the FACTSAGE Software to predict the predominant phase diagram of the Ni–O–H–Cl system at the typical SOFC operating temperature of 800 °C. The results as shown in Fig. 16 indicate the Ni phase remains stable until the concentration level of HCl is well above 100 ppm (as shown by the solid line at $\log_{10} P(HCl) = 1$). Furthermore, calculations performed on the YSZ electrolyte phase show similar results in Fig. 16 (as shown by the dashed lines). These analyses rule out the possibility for formation of stable bulk chloride phases on the SOFC anode during cell operation. Therefore it is more likely that chemisorption of HCl on the Ni particles accounts for the loss of cell performance over the 400 h period. The dissociatively adsorbed chlorine on the nickel surface may degrade cell performance in the following manner: firstly the chlorine can block the active TPB sites of the Ni–YSZ anode and thus incur additional polarization resistance for the electrochemical reactions. Secondly, as the bond between Ni and Cl tends to be more ionic than the covalent counterparts for reactions of sulfur on Ni [15], the adsorbed Ni–Cl species formed at the surface of the Ni particles can possess chloride-like properties such as low melting point and high-temperature volatility. These properties may cause gradual sublimation and re-distribution of Ni constituents at the near-surface region over the long-term. The SEM results show the

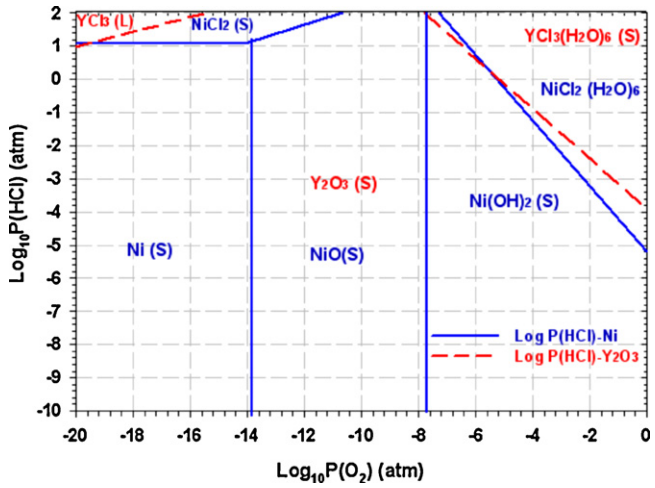

Fig. 16. Predominant phase diagram calculated for Ni–O–H–Cl system and Y–O–H–Cl system with a hydrogen partial pressure $P(H_2) = 0.3$ atm at 800 °C.

formation of scabrous Ni clusters on the surface of the Ni particles after HCl exposure, and the XPS results confirm the existence of Cl_{2p} peak at 197.20 eV as adsorbed chlorine on the anode. Hence, combining the experimental findings, the morphological change of the Ni–YSZ anode can be attributed to effects of chemisorption of HCl on the Ni surface. On the other hand, the cell degradation and microstructure evolution of the Ni–YSZ anode-supported cell seen here differ from the prior reports on chlorine poisoning of the SOFC anode for an electrolyte-supported cell. Haga et al. [3] found that the degradation of a Ni–ScSZ anode in H_2 fuel with chlorine was associated with the formation of $NiCl_2$ and its subsequent sublimation, resulting in significant loss of Ni from the anode. The reported phenomena of re-deposition of Ni nano-particles from the sublimation over the entire anode surface is not confirmed by our present results, since reconstruction of scabrous nickel was localized on the Ni particle surface only. Moreover, in our study the mole amounts of NiCl (g), $NiCl_2$, Cl (g) are significantly less than that of HCl at the SOFC working temperature in Ni–H–Cl–O system. Our observations are more in line with the results of Bao's group [4] who recently reported no significant degradation for exposure to 40 ppm HCl over 100 h. To reveal the HCl effect on the nickel catalyst, our exposed anode surface test protocol avoids the potential gettering effects of the nickel paste and current collector. Hence more detailed changes of the Ni–YSZ can be displayed on the post-mortem cell. An earlier study conducted by Trembly et al. indicated more severe degradation (voltage loss >15%) of a Ni–GDC anode on an electrolyte-supported SOFC operated with coal syngas containing 20 ppm and 160 ppm HCl [2]. One possibility leading to this variation of research findings may come from the thicker anode support configuration (~850 μm) and lower HCl level (100 ppm) utilized in the present study. As the impurity-containing syngas passes through the gas diffusion layer of the anode, HCl may be readily adsorbed on the surface of the Ni particles, reducing the amount of HCl actually reaching the anode/electrolyte active interface. Hence less degradation is observed in the present work because of low-coverage of chemisorbed chlorine on the Ni surface at the anode/electrolyte interface. SEM results support this assumption as it was shown that the morphology of the Ni particles at the anode surface tended to be more scabrous than that of the Ni particles at the anode/electrolyte interface deeper inside the anode.

In Fig. 13, the chlorine trace appears only on the Ni–YSZ cermet and not on the pure Ni and YSZ coupons. There may be two reasons for this result: (1) the electrochemical reaction occurs only in the Ni–YSZ cermet. There is no electrochemistry occurring on the Ni or YSZ coupons individually. The current flow may encourage adsorption of some chlorine on Ni–YSZ cermet as the fuel gas diffuses to the TPB. (2) Considering the surface area of these samples, the porous Ni–YSZ cermet has much higher surface area than that of the bulk Ni and YSZ coupons. The higher surface area of the Ni–YSZ cermet provides more active sites for the adsorption of chlorine on the Ni surface.

Earlier studies have identified sulfur (H_2S) and phosphorus (PH_3) as the most threatening impurities for the operation of Ni cermet SOFC anodes in coal syngas. Degradation caused by 5–100 ppm H_2S is mainly attributed to adsorption of sulfur on the Ni surface modifying the catalytic activity for electrochemical oxidation [16]. Also, 10 ppm phosphorus is sufficient to introduce secondary phosphide phases in the Ni-based anode accompanied by significant microstructural deterioration [5]. Current results for 100 ppm HCl impurity on anode-supported cells show that the poisoning effects on the Ni–YSZ anode are slower and much smaller in magnitude than the poisoning effects of sulfur. Unlike sulfur, an earlier study has shown that chlorine adsorbs mainly on the terrace 3-fold sites of Ni rather than the 4-fold sites [15]. The different chemisorption behaviors of chlorine and sulfur on the Ni surface may cause the different poisoning effects. The slight weight loss of Ni seen here within the relatively short testing duration is within the experimental uncertainty of the measurements. Hence, the need for longer term cell operation in syngas is required. If the loss of nickel is indeed occurring, HCl should be recognized as a potential menace to cell stability and system integrity.

5. Conclusions

A 400-h test of a Ni–YSZ anode-supported SOFC cell exposed to syngas with 100 ppm HCl contamination has been conducted. The degradation of cell performance (loss of voltage at constant current) was about 3% over the test period. This degradation is relatively less than that of reported in the previous literature [2,3], The cell series and polarization resistances remained almost constant during 400 h of testing. The results indicate that the anode-supported cell has higher tolerance of HCl impurity than the electrolyte-supported cell which had been tested by previous investigators [2,3]. The EDS data of the Ni–YSZ anode reveal that some loss of nickel concentration may occur due to attack of the Ni–YSZ anode by HCl in 400 h. Minor surface microstructural reconstruction of the Ni particles was observed in the SEM micrographs at 100K magnification. Traces of chlorine were found on the HCl-poisoned Ni–YSZ anode by XPS. The limited amount of Cl on the anode could be formed on the very surface of nickel particles by chemisorption processes at the SOFC working conditions. There is no evidence of the presence of nickel chloride compounds in the post-mortem Ni–YSZ anode. These findings suggest that the adsorption of chorine onto the surface of the Ni particles in the cell anode and the loss of nickel concentration are two related processes and both impact the cell performance. The loss of nickel is not significant in this study. However, it may have a more severe effect on the long-term durability of the SOFC power system, because it is an irreversible process.

The testing results also showed that 100 ppm HCl can severely corrode stainless steel tubing. Clearly, HCl in syngas poses a challenge not only to the tubing but also to any interconnects based on stainless steel or other corrodable materials. This issue cannot be ignored in SOFC systems using coal syngas.

Acknowledgements

This work is conducted under US DOE (Department of Energy) EPSCoR Program. It is jointly sponsored by US DOE Office of Basic Energy Sciences, NETL (National Energy Technology Laboratory),

WV State EPSCoR Office and the West Virginia University under grant number DE-FG02-06ER46299. Dr. T. Fitzsimmons is the DOE Technical Monitor. Dr. R. Bajura is the Administrative Manager and Dr. I. Celik is the Technical Manager and Principal Investigator of this project. The authors would like to thank Dr. R.S. Gemmen and Dr. Edward M. Sabolsky for suggestions and use of software. Dr. Andy Woodworth, Mr. Liviu Magean, Mrs. Andrienne McGraw are thanked for SEM, EDS, XRD and XPS data.

References

[1] J.P. Trembly, R.S. Gemmen, D.J. Bayless, Journal of Power Sources 163 (2007) 986–996.
[2] J.P. Trembly, R.S. Gemmen, D.J. Bayless, Journal of Power Sources 169 (2007) 347–354.
[3] K. Haga, Y. Shiratori, K. Ito, K. Sasakia, Journal of the Electrochemical Society 155 (12) (2008) B1233–B1239.
[4] JianEr Bao, G.N. Krishnan, P. Jayaweera, J. Perez-Mariano, A. Sanjurjo, Journal of Power Sources 193 (2009) 607–616.
[5] F. Zhao, A.V. Virkar, Journal of Power Sources 141 (2005) 79–95.
[6] C. Xu, J. Zondlo, H. Finklea, O. Demircan, M. Gong, X. Liu, Journal of Power Sources 193 (2009) 739–746.
[7] M. Yashima, S. Sasaki, M. Kakihana, Acta Crystallographica Section B 50 (1994) 663–672, Dec.
[8] M. Yousuf, P.C.H. Sahu, H.K. Jajoo, S. Rajagopalan, K. Govinda Rajan, Journal of Physics F 16 (1986) 373–378.
[9] D. Taylor, Transactions and Journal of the British Ceramic Society 83 (1984) 5.
[10] C.A. Tolman, W.M. Riggs, W.J. Linn, C.M. King, R.C. Wendt, Inorganic Chemistry 12 (12) (1973) 2770–2778.
[11] C.D. Wagner, W.M. Riggs, L.E. Davis, J.F. Moulder, G.E. Muilenberg, Handbook of Ray Photoelectron Spectroscopy, Perkin-Elmer Corporation, Physical Electronics Division, Eden Prairie, MN 55344, Section 8, 1979, pp. 2–3.
[12] G.M. Ingo, E. Paparazzo, O. Bagnarelli, N. Zacchetti, Surface and Interface Analysis 16 (1990) 515–519.
[13] J.C. Carver, G.K. Schweitzer, T.A. Carson, The Journal of Chemical Physics 57 (2) (1972) 589–1018.
[14] J.C. Klein, D.M. Hercules, Journal of Catalysis 82 (2) (1983) 424–441.
[15] H. Ishii, K. Asakura, T. Ohta, Y. Kitajima, H. Kuroda, Japanese Journal of Applied Physics 32 (2) (1993) 368–370, Supplement.
[16] M. Gong, X. Liu, J. Trembly, C. Johnson, Journal of Power Sources 168 (2007) 289–298.